# Single Molecule Kinetics of Styrene Hydrogenation on Silica Supported Vanadium: The Role of Disorder for One-Atom Catalysts

Robert H. Wells[1#], Suming An[1#], Prajay Patel[2], Cong Liu*[2], and Rex T. Skodje*[1]

1) *Department of Chemistry, University of Colorado, Boulder, CO 80309*

2) *Chemical Sciences and Engineering Division, Argonne National Laboratory, Lemont, IL 60639*

**Abstract:** A theoretical approach for the study of supported atom catalysis is developed based on recent advances in the study of single molecule kinetics. This view is particularly useful in exhibiting the role of disorder in single atom and single site catalysts on amorphous supports. The distribution of passage times (or waiting times) through a complex catalytic network originating from a set of coupled active sites is described by a probability distribution function, *f(t),* that reflects the local environment of the reaction center. An efficient algorithm is developed based on the linear algebra of the Markov transition matrix that produces *f(t)* or its moments. The kinetics of the hydrogenation reaction of styrene on an organovanadium(III) catalyst supported on amorphous silica is studied. A kinetic model consisting of three intertwined catalytic cycles emanating from three chemically distinct active sites is proposed to describe the chemistry. Density functional theory (DFT) calculations are employed to determine the free energy barriers of the reactions which are used to construct the rate coefficient matrix. The disorder induced by the amorphous support material is divided into a low-dimensional short-range component reflecting the covalent structures near the reaction center and a weaker long-range component modeling the bulk randomness. The results are computed and analyzed for a wide range of concentration values and disorder scenarios. Unusual structure in the *f(t)* probability distribution function (PDF) is found to occur for certain cases that reveal the contribution of multiple catalytic pathways acting in concert.

# Contributed equally to this work

# I. Introduction

Computational studies of the kinetics of surface catalyzed reactions have traditionally adopted an idealized surface chemistry that is a defect-free perfect crystal face environment. This greatly simplifies kinetic modeling since each catalytic site is assumed to be equivalent. In reality, inhomogeneity such as stepped faces, defects, roughness, and nanostructure[1-7] can greatly promote catalytic activity. Although many catalytic environments are disordered,[8-10] it is difficult to theoretically model the activity of such systems. The large number of required quantum chemical calculations needed to represent chemical barriers over the distributed environments are burdensome to carry out. There are also ambiguities about how the random environments should be selected. Furthermore, it is not trivial to model the full kinetics of the system even provided the distribution of energetic barriers. Of interest here are single site and single atom catalysts that are important cases where the microscopic environment can play a decisive role in the kinetics.[11 12] Amorphous supported catalysts are interesting due to the large degree of heterogeneity in the catalytic environment. A common amorphous support, $SiO_2$, shows heterogeneity in catalytic sites due to non-uniform bonding of the metal atom to the support and dangling silanol groups that can be stretched or angled towards the metal catalytic atom. These variations can be responsible for a distribution of reaction barriers during catalysis. This was investigated in the work of Peters, Scott and co-workers[13 14] who examined the statistical effects of amorphous supported catalysts with distributed energy barriers. They concluded that a small percentage of catalysts that possess the lowest activation energy may be responsible for the majority of catalytic events. However, how to rigorously treat the disorder of the system remains an unresolved issue. We note that using methods such as the degree of reaction control,[15 16] global sensitivity analysis,[17 18] and the De Donder relations[19] it is possible to assess the relativity importance of specific barriers in the overall catalytic turnover. Such sensitivities may reveal particularly critical steps in a model and can provide insight in assessing wherein the disorder may have the greatest impact.

Modeling the kinetics of a disordered system requires an explicit scheme to set rate coefficients, usually by assigning barrier energies and using transition state theory (TST). For single reactions, one can imagine a probability distribution of barriers which yields a distribution of rates via TST. For more complicated multistep reaction networks, we must face the question: are the random uncertainties of individual barrier energies correlated to each other, or are they

independent random variables? A computationally intensive approach is to create a large ensemble of random structures from a large atomistic representation of the support, perhaps using annealing, and computing all the barrier energies using quantum chemistry for each locally optimized structure.[20] In lieu of this massive calculation, we adopt a simpler approach based on the idea of dividing the disorder into local and global components. For a covalently bonded system, we can imagine the local environment determined by a small number of structural features in the immediate vicinity of the reaction center which can be parameterized by a small number of geometrical factors $\boldsymbol{r}$, i.e., bond lengths, bond angles, and so forth. Fixing $\boldsymbol{r}$ sets a local constraint[21] and the remaining geometries are optimized. The long-range disorder is due to structures distant from the reaction center and is very high dimensional, $\{\boldsymbol{\sigma}\}$, which may be approximated as noise. The probability distribution of barriers is highly correlated for local structure, but uncorrelated for long-range structure. Thus, if there are n-energetic barriers and wells in the reaction network, $\boldsymbol{E}$, they are functions of $\boldsymbol{r}$ up to additive random noise, i.e., $\boldsymbol{E=E(r)+\Delta(\{\sigma\})}$. This reduces the complexity of the model by requiring knowledge only of the probability distribution of the local structures. This idea in the limit of zero noise was introduced in an earlier work on $SiO_2$ supported single metal-atom catalysts where just one bond length was used to model local disorder.[22] To model disordered kinetics, we need to compute observables such as the turnover frequency for potentially large reaction networks that sample the values of the disorder parameters. Because the observables themselves are also functions of many parameters, i.e. concentration and temperature, this requires an enormous number of kinetic simulations. Since analytic expressions cannot be relied on for complex networks, a numerical approach is required. Conventional kinetic Monte Carlo simulation is a candidate method we also have employed,[22] but it is still quite slow numerically. Instead, here we introduce a matrix-based method that uses efficient singular valued decomposition (SVD) manipulations to extract the observable properties of the catalyst.

One very useful way to investigate disorder in a catalytic system employs the concepts and methods of single molecule kinetics where reactivity is resolved at the single molecule level. [23-27] These techniques are especially informative since they reveal the differences in kinetics occurring in various microscopic environments. Some of the earliest investigations involved enzymatic catalysis where the activity was correlated strongly with the enzyme's conformational structure. The biophysical community has made impressive progress in developing both the experimental

methodology and the theoretical framework to gather and interpret the experimental data.[28 29] Many applications of this technology clearly establish that single molecule kinetics is a useful tool to unravel the role of local environment on chemical reactivity.[30-41] Of particular interest here is the work of Chen and coworkers who have observed catalysis occurring on single nanoparticles and developed a real-time description of individual product formation.[42-48] These studies have yielded intriguing descriptions of the kinetics and give a convenient framework that naturally extends to amorphous systems. In the present context of single atom catalysis, each active site embedded onto the amorphous support can be occupied by only one reactant molecule or intermediate at a time. Single atom turnover frequencies (TOF's) are then collected for each distinct environment. The turnovers are typically quantified by the waiting time probability distribution functions, $f(t)$, that records the formation and release of individual product molecules from a site and reflect the full kinetic mechanism operating at the site. The bulk TOF is an average over the single sites, but the single molecule results are vastly more informative.

In this work we explore the single molecule view of the kinetics of a single site organovanadium(III) catalyst supported on amorphous silica, specifically we treat the hydrogenation of styrene in a nonpolar solution to yield the product ethylbenzene. The chemistry of alkene molecules on such catalysts has been explored in detail experimentally. [49-51] A reaction mechanism was proposed in an earlier work[22] that was guided by experimental results for a related alkene, butylstyrene, and by insight into behavior of amorphous silica.[52-54] Nevertheless, several unresolved issues remain, not the least of which is the role of disorder of the amorphous environment in the activity of the catalyst. In the model, the local disorder in the system is parameterized by a single bond length between the vanadium and the support. While this one-dimensional parameterization is clearly an oversimplification, we believe the outline of the approach is a good first step in understanding how disorder impacts the activity of the catalyst.

# II. Kinetic modeling of bulk and single atom catalysis

## A. Bulk kinetics

A common kinetic description of a bulk phase catalytic reaction employs the Michaelis-Menten mechanism (MM).[55 56] In the simplest version, a single site catalyst E converts a substrate S to a product P through a single intermediate complex ES via the mechanism

$$E + S \underset{k_{\pm 1}}{\longleftrightarrow} ES \underset{k_2}{\rightarrow} E + P$$

where the release step is assumed to be irreversible. The model is solved at low E concentrations, $E_0 = [E] + [ES]$, under steady state conditions to obtain the turnover frequency (TOF)

$$\nu = \frac{k_2[S]}{[S] + K_M} \quad with \quad K_M = \frac{k_{-1} + k_2}{k_1} \tag{2.1}$$

which is related to the overall reaction velocity by $vel = [E_0]\nu$. The TOF of these models exhibits hyperbolic saturation phenomenon at large [S], i.e., $\nu \rightarrow \nu_{max} = k_2$ as $[S] \gg K_M$, and a linear Lineweaver-Burk plot of $\frac{1}{\nu}$ $vs$ $\frac{1}{[S]}$. It has been demonstrated that the average of the single molecule TOF, under many circumstances, will likewise show saturation behavior with a generalized description of the physical meaning of the MM parameters $\nu_{max}$ and $K_M$.[33]

Simple analytical behavior can sometimes be obtained for more complicated catalytic motifs than the basic MM scheme, although the expressions for $\nu_{max}$ and $K_M$ must be generalized and perhaps include inhibitor concentrations.[56] [57] [58] These motifs may yield to hyperbolic or more complicated saturation curves. When more the one substrate is involved, as in the present case, the MM formula must be generalized to account for multiple substrate concentrations. A class of models for two concentrations (*[A]* and *[B]*) is described by the TOF expression[56]

$$\nu = \frac{\nu_{max}[A][B]}{[A][B] + K_{MA}[B] + K_{MB}[A] + K_{iA}K_{MB}} \tag{2.2}$$

where $K_{MA}$ and $K_{MB}$ are Michaelis constants for attachment of A and B substrates and $K_{iA}$ is an equilibrium constant for E+A↔EA. When the catalytic motif is complicated by inhibition, multiple substrates, multiple active sites, and disordered structural environments, the TOF is difficult to analytically represent in any useful way and a numerical approach is preferred.

B. Single molecule kinetics

The single molecule view of kinetics is well adapted to treating the behavior of supported single atom catalysts.[59] The great advantage of this viewpoint is that the total kinetic turnover can be straightforwardly decomposed into a convolution over the distinct environments. Experimentally, detailed observations can directly resolve the activity of single enzymes or

nanoparticles in their distinct structures. Theoretically, the activity of a single environment such as a structure can be predicted from reaction energetics. The fundamental descriptor in single molecule catalytic kinetics is the probability distribution function (PDF) of reactive waiting times from a single active site, $f_q(t)$. The waiting time $t$ is defined as the time interval between the catalytic turnover cycles from one catalytic molecule or atom and is the sum of times for each step along the pathway leading to product release. The label $q$ denotes distinct structures of the catalyst which models the disorder. For a simple sequential cycle, a single catalytic atom E processes a substrate S to product P through a set of n intermediates $(ES)_i$ arranged along a linear chain, $E + S \leftrightarrow (ES)_1 \leftrightarrow (ES)_2 \leftrightarrow \cdots (ES)_n \rightarrow E + P$; there, the event time $t$ is measured between sequential product release reactions $(ES)_n \rightarrow E + P$. No new substrate can bind to E during the sequence which requires passage through the full cycle to renew. More generally, a full cross-linked reaction network will govern the catalytic turnover at the active site. The turnover frequency (TOF) from a single site, $\nu_q$, is obtained from the first moment of the PDF, $\langle t \rangle_q = \int_0^\infty t \cdot f_q(t)\, dt$,

$$\nu_q = \frac{1}{\langle t \rangle_q} \qquad (2.3)$$

The $f_q(t)$ for site $q$ is obtained by simulating the kinetics for the reaction network that take reactants to products using the rate coefficients appropriate to structure $q$. The observed TOF of a macroscopic sample of many inequivalent AS's is then obtained by the average

$$\nu_{obs} = \sum_q F_q \nu_q \qquad (2.4)$$

where $F_q$ is the probability of the structure $q$ in the sample. This relation assumes a static distribution so that each TOF may be computed from a single set of rate coefficients. In the present case, the chemistry is due to a single vanadium atom and distinct catalytic atoms in the sample do not communicate. We shall distinguish two varieties of active site (AS) distributions, structural and chemical. In the present supported V-atom problem, the structural distribution corresponds to various amorphous configurations of the $SiO_2$ support which is assumed to be rigid and static on the time scale of the experiment. The chemical distribution refers to distinct chemical structures for the AS that may develop from the pre-catalyst. Here, these are associated with different ligands on the V-atom that yield different catalytic cycles but with the same rigid amorphous structure of $SiO_2$. The chemical distributions may interconvert on the experimental time scales and must be

treated on par with the other catalytic chemistry. Should the $SiO_2$ structures become nonrigid, the distinction between chemical and structural configurations blurs.

We model the catalytic network assuming the intermediate species $X_i^q$ interconvert through the pseudo-first-order reactions, $X_j^q \rightarrow X_i^q$ with rates given $k_{i,j}^q[X_j^q]$. The concentrations of the substrates, styrene, and $H_2$ in the present case, or inhibitors, THF in the present case, are taken as constant parameters within $k_{i,j}^q$. The rate coefficients for the reaction step j→i is given by the standard Eyring form, $k_{i,j}^q = \frac{k_B T}{h} e^{-\Delta G_{i,j}^{\ddagger,0}(q)/k_B T} \cdot Z$ where Z is either [ST], [$H_2$], [THF] or 1 depending on the reaction and $\Delta G_{i,j}^{\ddagger,0}(q)$ is the structure-dependent standard free energy barrier for $j(+Z) \rightarrow \ddagger \rightarrow i$. The free energies are provided by the DFT calculations and include energetic and entropic contributions, and in principle may also include solvation effects.

C. Stochastic Modeling:

We assume the catalytic network consists of N distinct species including m chemically distinct AS's. We represent each of the N chemical species in the catalytic network as a "state" in a continuous time Markov stochastic process with occupation probability $P_i(t)$, $i$=1,…,N+m.[60 61] We have augmented the state space to include the m AS's as both initial and final states for mathematical convenience. The AS's may interconvert via first order kinetics on the same footing with other reactions in the network. Thus, all species are combined into a single state vector that includes both the initial and final states of the AS's. (For the moment we drop the cumbersome "$q$" superscripts which are implicit in all the probabilities and rates.) The first m states are taken as the reagent states, i.e., $E_i$+Reactants, and the final m states are the product states $E_i$+Products, with i=1,…,m. Here, the $E_i$'s are the m chemically distinct AS's. Importantly, we assume the final m product Markov states are "absorbing" so that all reactions into them are irreversible, $k_{j,N+i} = 0$ with $\mathrm{i} = 1, \ldots, \mathrm{m}$ and $\mathrm{j} = 1, \ldots, \mathrm{N} + \mathrm{m}$. This is strictly valid only in the limit of zero product, i.e., for the initial stages of reaction. The first N states are termed "transient" since any molecule lying in those states will eventually transition into the absorbing states after some amount of time. The rate coefficients in the Markov chain picture are then state-to-state transition probabilities per unit time. The time evolution of the state probabilities is given by the familiar system of first-order ordinary differential equations (ODEs) in terms of the probability vector $\boldsymbol{P}=(P_1, \ldots, P_{N+m})$ and the $(N+m) \times (N+m)$ transition rate matrix $\boldsymbol{G}$ (also known as the generating matrix)

$$\frac{d\boldsymbol{P}(t)}{dt} = \boldsymbol{G} \cdot \boldsymbol{P}(t) \qquad (2.5)$$

where

$$\boldsymbol{G} = \begin{pmatrix} -k_1 & \dots & k_{1,N+m} \\ \vdots & \ddots & \vdots \\ k_{N+m,1} & \dots & -k_{N+m} \end{pmatrix} \qquad (2.6)$$

The diagonal elements $G_{i,i}$ for i=1,…,N are the (negative) decay probabilities per unit time of state i, $k_i = \sum_{j=1}^{N+m} k_{j,i}$ for i=1,..,N. Each column of the matrix sums to zero reflecting conservation of probability. The last m columns of $\boldsymbol{G}$ are zero since transitions out of the absorbing states are forbidden. The solution of this system models the first passage time from the initial state $\boldsymbol{P}(0)$ to any final absorbing state and the waiting time PDF is given by the derivative of the total final state probability for all the final product states, i.e.

$$f(t) = \sum_{i=1}^{m} \frac{dP_{N+i}(t)}{dt} \qquad (2.7)$$

In our previous work,[22] we modeled the single molecule kinetics of eq. (2.5) using a kinetic Monte Carlo scheme in which an ensemble of similarly prepared sites was propagated using methods similar to those proposed by Gillespie.[62] [63] Here, for the most part, we adopt a more computationally efficient approach based on linear algebra.

Further analytical progress on this problem is possible[61] **Error! Bookmark not defined.** by partitioning the generating matrix $\boldsymbol{G}$ into a sub-generator $\boldsymbol{T}$ and an absorption matrix $\tau$

$$\boldsymbol{G} = \begin{pmatrix} \boldsymbol{T}_{N\times N} & \boldsymbol{0}_{N\times m} \\ \boldsymbol{\tau}_{m\times N} & \boldsymbol{0}_{m\times m} \end{pmatrix} \qquad (2.8)$$

where

$$\boldsymbol{T} = \begin{pmatrix} -k_1 & \dots & k_{1,N} \\ \vdots & \ddots & \vdots \\ k_{N,1} & \dots & -k_N \end{pmatrix} \qquad (2.9)$$

and

$$\boldsymbol{\tau} = \begin{pmatrix} k_{N+1,1} & \cdots & k_{N+1,N} \\ \vdots & \ddots & \vdots \\ k_{N+m,N} & \cdots & k_{N+m,N} \end{pmatrix} \qquad (2.10)$$

Physically, $\boldsymbol{T}$ represents transitions between the transient states while $\tau$ describes transitions from transient states into absorbing states. By conservation of probability $\sum_{i=1}^{N+m} G_{i,j} = 0$ implying that $\sum_{i=1}^{N} T_{i,j} = -\sum_{i=1}^{m} \tau_{N+i,j}$ for j=1,…,N. In other words, the net transition rate out of a transient state j to other transient states i≠j equals negative of the transition rate of j into the absorbing states. The passage time through the network is determined by $\boldsymbol{T}$ and does not require the redundant specification of $\boldsymbol{\tau}$. The sub-generator $\boldsymbol{T}$ is an invertible matrix (unlike $\boldsymbol{G}$) and it can be shown that the moments are obtained by matrix inversion[61]

$$\langle t^n \rangle = n!\, \mathbf{1}^{\boldsymbol{T}} \cdot (-\boldsymbol{T})^{-n} \cdot \boldsymbol{P}(0) \qquad (2.11)$$

In particular, the TOF is given by the first moment

$$\nu = \frac{1}{\mathbf{1}^{\boldsymbol{T}} \cdot (-\boldsymbol{T})^{-1} \cdot \boldsymbol{P}(0)} \qquad (2.12)$$

and the full waiting time distribution is

$$f(t) = \mathbf{1}^{\boldsymbol{T}} \cdot (-\boldsymbol{T}) \cdot \exp(\boldsymbol{T}t) \cdot \boldsymbol{P}(0) \qquad (2.13)$$

The vector $\boldsymbol{1}^T$ is the transpose vector of all one's and $\boldsymbol{P(0)}$ is the initial state vector, which is some distribution over the active sites. The TOF for the site is then obtained from the first moment without the need for explicit time propagation.

If there are m-chemically distinct AS's, there will be m potential "initial states" and m potential absorbing "final states". We require a method to set $\boldsymbol{P(0)}$ when the system is in steady state which occurs after many turnovers. To achieve stationarity, the total decay rate from a specific initial state must be equal to the formation rate of the corresponding absorbing state. Hence, we have the steady state conditions

$$k_i P_i(0) = \sum_{j=i}^{N} k_{N+i,j} P_j(0) \;\; i = 1, \ldots, m \qquad (2.14)$$

These homogeneous equations can be solved using the constraint $\sum_{i=1}^{m} P_i = 1$ . If the active sites rapidly interconvert the initial state can be approximated with the equilibrium constants.

The standard difficulty that arises with the stochastic matrix approach is the possibility of ill-conditioned transition matrices for certain regions of parameter space.[61] As a result, an unacceptable level of noise may occur in the evaluation of observables in those regions. This difficulty is usually dealt with by invoking a preconditioning process on the linear system that lowers the effective condition number of the matrix. A quasi-equilibrium approximation can accomplish the same thing by eliminating certain rapid steps from the mechanism.

### D. Kinetic Monte Carlo

The single molecule perspective is based on solving the eqs. (2.5)-(2.7) for the waiting time distribution *f(t)* by any consistent method. An alternative to the matrix method of Sec. II.C is to use the stochastic simulation method of Gillespie[62] to generate the first passage time through the network using an explicit random walk algorithm. We refer to this as the kinetic Monte Carlo algorithm, kMC. The problem manifested by high matrix condition number in Sec. II.C is here exhibited through very long required propagation MC flights due to a separation of time scales between reactions with very different barrier heights. This problem can be ameliorated by invoking a quasi-equilibrium approximation. Thus, if two or more species rapidly interconvert but decay slowly as a group, we can equilibrate the concentration within that family; e.g. if $X_1 \underset{k_f,k_b}{\longleftrightarrow} X_2$ is rapid then $\frac{[X_2]}{[X_1]} \approx \frac{k_f}{k_b}$ and the fastest transition can be dropped from the list of potential MC events. This well-known approach[62] accelerates the calculation considerably and can be used sometimes when the ill-conditioning problem of the matrix method is severe.

# III. Hydrogenation of Styrene on Vanadium Catalysts

## *A. Chemical model*

The modeling catalytic kinetics of styrene hydrogenation requires detailed information about the nature of the AS's and rate coefficients of the steps along the catalytic cycles. In a previous work,[22] the model based on quantum chemistry and chemical insight was described in detail which here we briefly review. The model was generated from electronic structure

calculations using Gaussian16[64] software and guided by experimental studies of 4-butylstyrene hydrogenation catalysis on the same surface. For the amorphous $SiO_2$ support, silsequioxane cages composed of siloxane ring structures were used in place of periodic DFT calculations. To model top monolayer relaxation in periodic models, the bottom half of the silica cluster (6 H, 11 O, and 6 Si atoms) was kept frozen during the optimization and frequency calculation. Styrene (ST) was used as the model reactant. All structures were optimized using the B3LYP density functional[65 66] and CEP-31G pseudopotential double-ζ basis set.[67 68 69] The thermal corrections to the Gibbs energy profile are done for 50°C and the frequency determination are made using B3LYP with the TZVP[70] basis set. It is assumed that solvent effects are small and are ignored.

In the experimental analog system involving 4-butylstyrene, the active sites on the catalyst evolve from a pre-catalytic surface where a single $V^{III}$ atom was tethered to the surface by several V-O bonds and capped with ligands Mes(mesitylene) and THF (tetrahydrofuran).[51] The surface

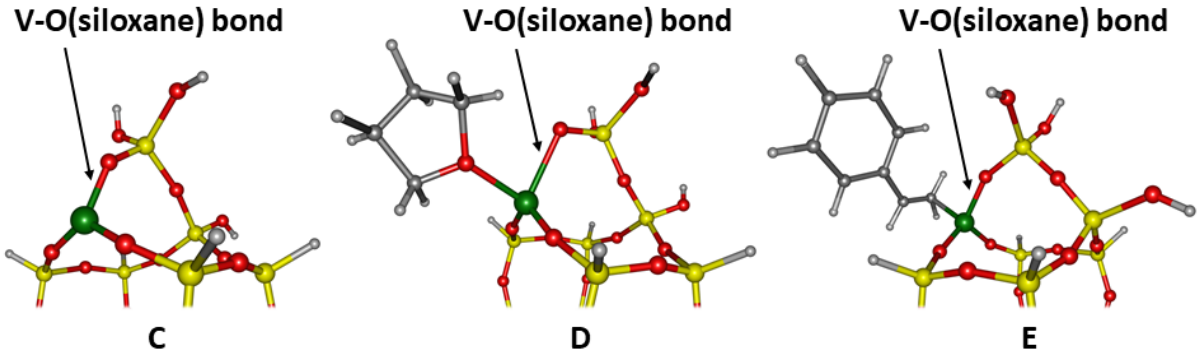


*Figure 1. The structures of three potential active sites. The vanadium atom (green) is tethered to the $SiO_2$ support by bonds to the silsequioxane cage. The vanadium atom has no ligand in the first structure, a ligand THF in the second, and a ST ligand in the third. One of the V-O bond lengths is systematically altered in each structure to simulate short-range disorder.*

was pretreated by exposure to $H_2$ that leads to three feasible active sites where some or all of the ligands were removed. These structures are pictured in Fig. 1, labeled C, D, and E. These correspond to V-atom ligands: bare, THF, and ST, respectively.

The chemistry of the system involves two substrate species, styrene (ST) and hydrogen ($H_2$), an inhibitor (THF), and three active sites. Three interlaced chemical pathways were identified

that accomplish the overall reaction Stryene+$H_2$→Ethylbenzene which are shown in Fig. 2. The active sites can interconvert by reversible attachment of THF and ST from solution.

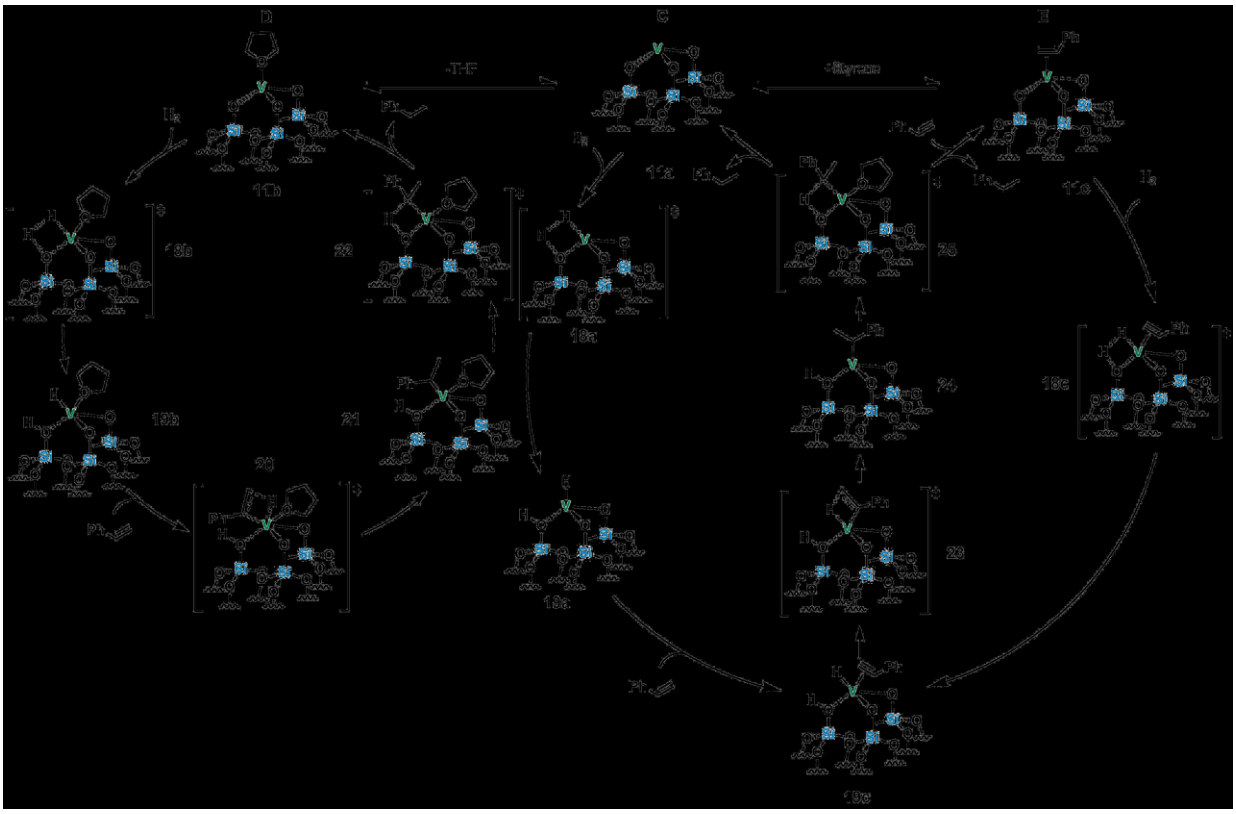

*Figure 2. The proposed catalytic scheme. The three active sites can interconvert by attachment/detachment of ST of THF to the V-atom. The scheme involves three interconnected cycles (or pathways). The transition state structures are indicated in brackets. Reprinted with permission from Ref 22. Copyright American Chemical Society.*

As seen in the diagram, the catalytic cycles are connected, through (i) ligand attachment/detachment of the active sites, (ii) at the merging structure **19c**, and (iii) at the branching structure **25**. The free energy profiles that emerge from the assumed optimized $SiO_2$ developing from the pre-catalytic structure are shown in Fig. 3. We note that the barriers for the reactions $D \leftrightarrow C \leftrightarrow E$ and $\mathbf{19}\boldsymbol{a} \leftrightarrow \mathbf{19}\boldsymbol{c}$ are significantly lower than the others and are amenable to a quasi-equilibrium approximation. There are 10 stable chemical structures and 9 transition states that contribute to this mechanism. The $\boldsymbol{T}$ matrix above is thus a 10×10 matrix and the $\boldsymbol{G}$-matrix, augmented with the absorbing states is 13×13. The concentrations of ST, $H_2$, and THF enter the $\boldsymbol{T}$-matrix as multipliers of the rate coefficients and should be expressed in molar units in keeping with the definitions of the standard free energies. Hence, the matrix is parameterized by

the vector ***X***=(ST, $H_2$, THF), i.e., ***T(X)***. It is not obvious whether the TOF for this catalytic model would be described by a simple parameterization such as that of eq. (2.2).

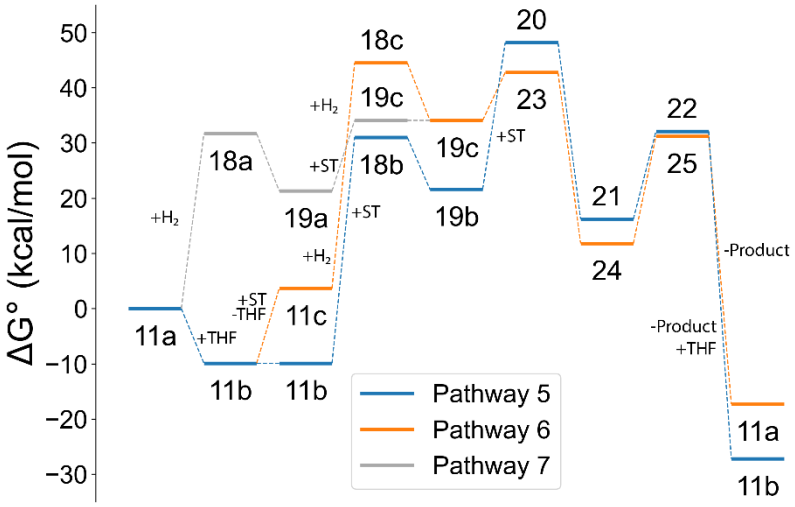


*Figure 3. The free energy for the structures shown in Fig. 2 relative to active site C. The pathways 5, 6, and 7 are indicated with blue, orange, and gray connecting lines, respectively. The nominal temperature is 50°C and concentrations are 1M.*

## *B. Structural Disorder*

In the previous report,[22] we introduced a simple model for the structural disorder of silica in this system. Here we briefly describe this model. The coordination environment of the V site is essentially determined by a set of structural parameters, such as V-O bonds and O-V-O angels, etc. For this class of supported organometallic catalysts, amorphous silica is used, which has no facets, but yet numerous local environments lead to the heterogeneity of the grafting sites. The resulting V sites also have a variety of coordination environments. Here we simplify the structural parameters to a single parameter, one of the V-O bond distances, and use the change of this parameter to mimic the heterogeneity of the active sites. While other geometric parameters, such as bond angles and dihedrals, as well as the distance between two ≡SiO− groups, could play a role in describing the relative position of the siloxane, the V-O (siloxane) distance is an effective simplification that is sufficient to demonstrate a qualitative trend in catalysis (*vide infra*). Based on the DFT optimized V-O distance for 1c (2.29 Å) in the fully relaxed model coming from the pre-catalyst, three rigid V-O (siloxane) distances are considered: *2.1*, *2.3* and *2.5* Å as representative structures for compressed or elongated local environments in an amorphous silica surface. These distances are both chemically feasible in an amorphous sample and had a critical

impact on the effective turnover frequencies. The four representative structures for the catalytic pathways corresponding to each individual V-O(siloxane) distance, i.e., fully relaxed (2.29 Å), 2.1, 2.3, and 2.5 Å, represent two scenarios of surface heterogeneity: one that utilizes the rigidness of the neutral siloxane groups on the surface of amorphous silica, which infers the positions of the siloxane relative to the metal center, and the possibility that the donor siloxane could be on the edge or corner of the amorphous silica sample, which could provide more flexibility for the siloxane donor during grafting and catalysis given the extra degrees of freedom. As the V-O bond length is extended to distances larger than 2.5Å, the energy of the active sites grows large and presumably sites with such values become very improbable.

The energetics of the chemical model of Fig. 2 were computed at a series of fixed values of one V-O bond length, *r*. This V-O bond refers to the bond between the V center and the siloxane group, shown by the arrow in Fig. 1, is held fixed away from its optimum value and the remaining chemical geometries and energetics are optimized subject to that constraint. Thus, a particular $SiO_2$ structure was first chosen as a fiducial based on the pre-catalyst, and other members of the disordered sample were represented as a one parameter family. The energetic profiles along catalytic pathways for the four values of *r* computed are shown in Fig. 4.

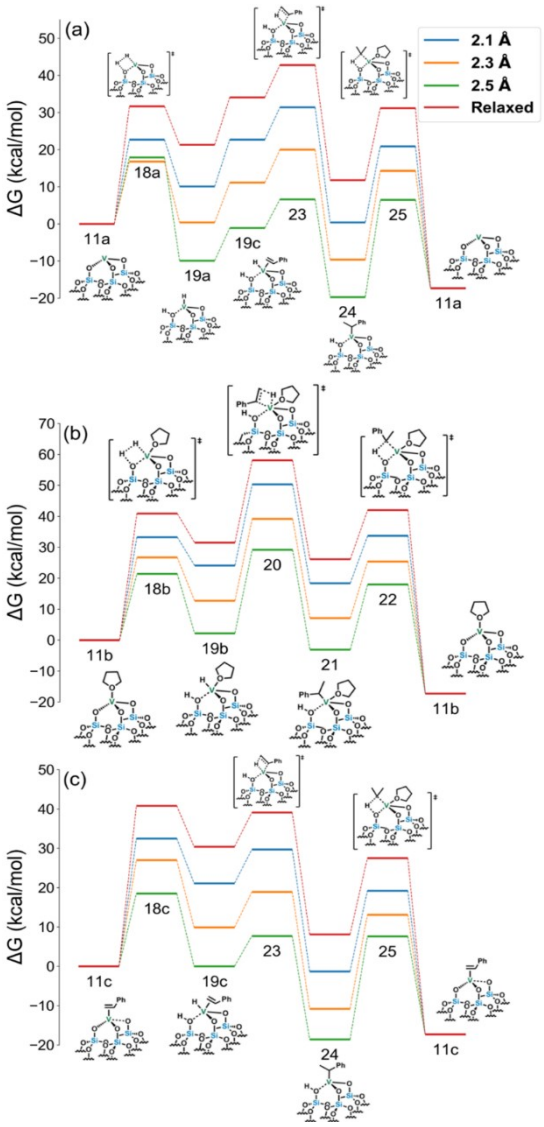


*Figure 4. The free energy profiles along pathways (a) 5, (b) 6, and (b) 7 computed as a function of the parameter r (V-O bond length) used to model short-range disorder in the sample. Reprinted from Ref. 22 with permission, Copyright American Chemical Society.*

In the rate computations, we have used a cubic spline interpolation scheme to obtain each barrier and well energy as a continuous function of *r.* Hence the transition matrix itself is also a function of the parameter *r*, i.e., $\boldsymbol{T}(r)$, as is the TOF, $\nu(r)$. If the probability distribution of *r* is denoted by $F(r)$, then the observed TOF via eq. (2.12) is

$$\nu_{obs} = \int F(r)\nu(r)\,dr = \int F(r)\left[\mathbf{1}^{\boldsymbol{T}} \cdot \left(-\boldsymbol{T}(r)\right)^{-1} \cdot \boldsymbol{P}(0)\right]^{-1} dr \qquad (3.1)$$

In addition to the short-range disorder modeled by the one-parameter family of V-O bond lengths,

we also consider the possibility of long-range disorder induced by more distant structural randomness. This was represented by a Gaussian random noise function with variance $\sigma^2$ which was added to the energy of each barrier and well in the chemical model. There was no correlation between the added noise at the various stationary points and the variance was assumed to be the same for all values of *r*. The observed TOF is an average of $\nu$ computed from a random sample of barriers and wells at each *r*, so that

$$\nu_{obs} = \int F(r)\langle \nu(r) \rangle \, dr = \int F(r) < \left[ \mathbf{1}^{\boldsymbol{T}} \cdot \left( -\boldsymbol{T}(r) \right)^{-1} \cdot \boldsymbol{P}(0) \right]^{-1} > dr \qquad (3.2)$$

At present it is not clear what the distribution *F(r)* should be nor is the value for the noise parameter σ (although see Sec. VII). We note that eq. (3.2) is easily generalized to include more than one local disorder parameter, should that information be available, specifically $r \rightarrow \boldsymbol{r}$ and $dr \rightarrow d^n r$.

# IV. Results for Turnover Frequencies

The matrix methods described above are efficient and make it possible to generate results for many thousands of parameter values of [ST], [$H_2$], and [THF] even including disorder. The results presented here are meant to give a survey of the qualitative trends predicted by the model and not a direct representation of experimental results which do not exist at present for styrene reactions but only for butylstyrene. Hence, we choose values for convenience.

We first illustrate the turnover frequencies obtained at fixed values of *r* computed without noise as functions of the concentrations [ST], [$H_2$], and [THF] in Fig. 5. We select a temperature of 325K to present results and the matrix inversion was carried out using the SVD. The waiting time distribution is found to be extremely insensitive to the choice of initial state, ***P(0)***, since the active sites C, D, and E rapidly equilibrate before the first (slow) $H_2$ attachment step. In Fig. 5a-c we show the TOF, $\nu$, versus *r* under a number of conditions. There is clearly an optimal range of values near r=2.36Å where $\nu$ reaches a maximum, while at small *r* values the catalyst is relatively inactive due to higher barriers. In Fig. 5e, we show $\nu$ versus [ST] for several values of [THF] at an optimal *r* value. The results exhibit typical saturation behavior versus [ST] at fixed values for the remaining parameters. Also, in Fig. 5g, are the corresponding linear Lineweaver-Burk plots of $\frac{1}{\nu}$ $vs$ $\frac{1}{[ST]}$ from which the MM parameters may be extracted. However, it is found that the values of the MM parameters can vary dramatically as a function of *r* and at some values we can see clear

departures in a linear Lineweaver-Burk plot. It is clear from Fig. 5g that the THF acts as a noncompetitive inhibitor since the straight lines do not intersect at $\frac{1}{\nu} = 0$ but instead occurs at some negative value. The TOF versus [$H_2$], Fig. 5d, also shows saturation behavior for low values of [THF]. When [THF] is large or when *r* lies significantly below the optimum value, we observe a linear dependence of ν on [$H_2$] or [ST] for all reasonable concentration values since the predicted Michaelis parameter ($K_M$) is extremely high. The TOF versus [THF] is shown in Fig. 5f for several values of [ST]. There is clearly strong inhibition of the TOF due to THF. For [$H_2$], THF acts more in keeping with competitive inhibition as $\frac{1}{\nu}\ vs\ \frac{1}{[H_2]}$ seem to intersect near $\frac{1}{[H_2]} = 0$. Thus, in

summary, the performance of the catalyst is found to have a strong *r*-dependence with respect to all the controllable parameters of the system.

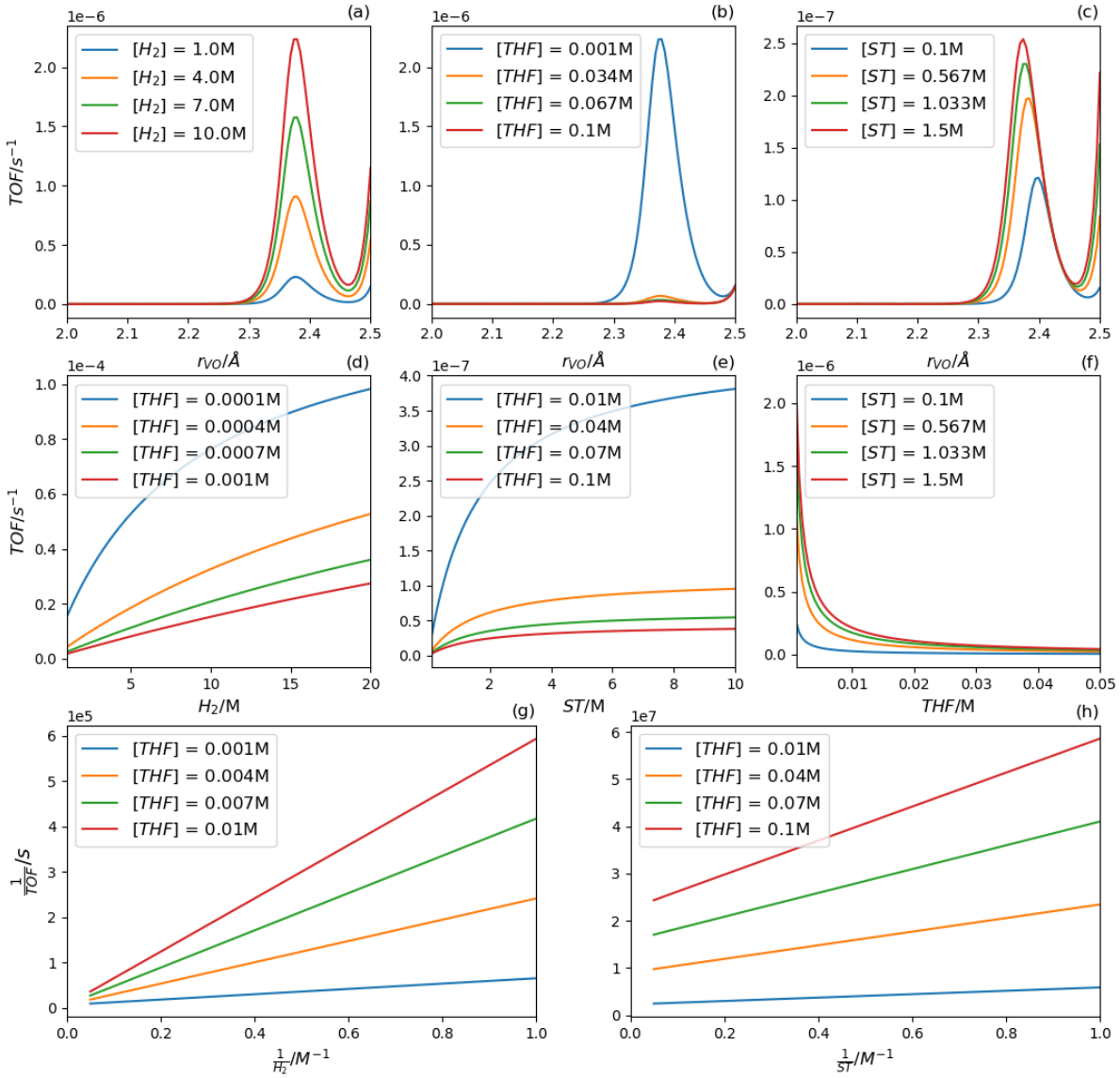


*Figure 5. The TOF (ν) at T=325K computed using eq. (2.12) for various values of the system parameters. Panels a-c show the r-dependence of ν for various values of [H₂], [THF], and [ST] respectively. In d-f the concentrations dependencies of ν are shown for the H₂, ST, and THF at r=2.36Å. In g and h, the Lineweaver-Burk plots are shown for H₂ and ST at r=2.36Å*

To fully account for the structural disorder in a bulk sample to obtain $\nu_{obs}$, it is necessary to average the TOF over both $r$ (short-range) and $\sigma$ (long-range) disorder as in eq. (3.2). Here our purpose is to qualitatively explore the sensitivity of the kinetics to the disorder so we simply test several potential distributions. First, we consider the influence of Gaussian noise on the TOF at

fixed values of $r$. The concentrations were held fixed at [ST]=1M, [$H_2$]=5M, and [THF]=0.01M and the TOF was computed for the reaction networks for 500,000 random values for the additive noise added to the barriers and wells. The calculation is repeated over a range of fixed $r$ for a number of values of the StDev $\sigma$. As shown in Fig. 6, the noise can increase the TOF by up to an order of magnitude at reasonable values of $\sigma$. Clearly, the more active catalysts (with lower activation barriers) are emphasized in the average as noted by Peters et al.[13] We note that, while the activity of the site seems to continue to grow at beyond r=2.5Å, the probability of such sites in the sample decreases rapidly due to the high energy of such structures.

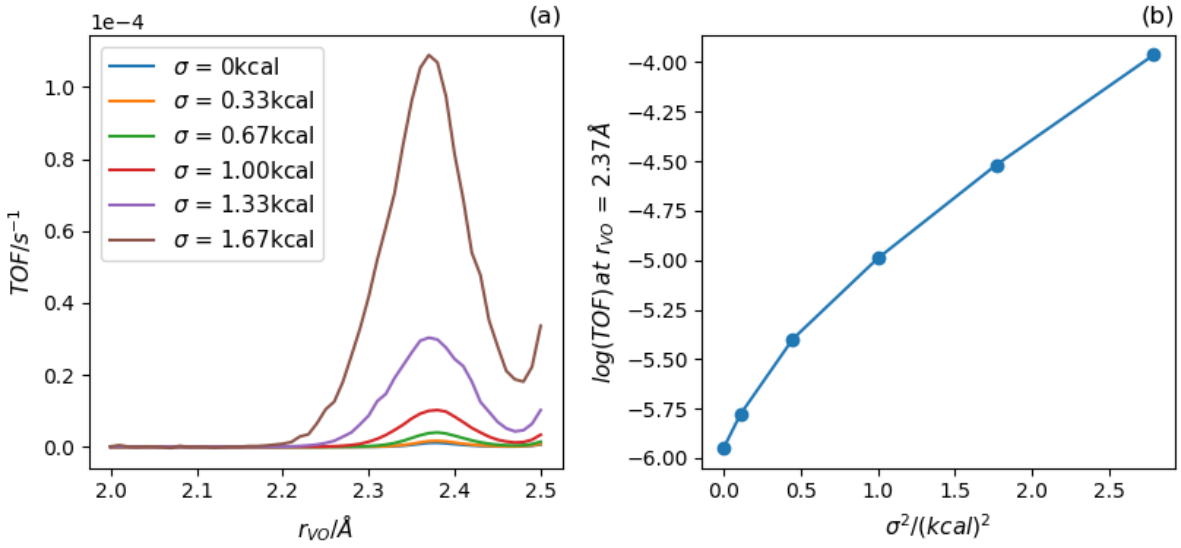


*Figure 6. The TOF at computed for T=325K, [ST]=1M, [$H_2$]=5M, and [THF]=0.01M with the addition of random Gaussian noise to each barrier and each well free energy for a number of values of σ. In (a) the TOF is shown as a function of r, and in (b) the TOF at the near optimal value of r=2.36 Å is plotted versus the variance $\sigma^2$.*

The averaging over short-range disorder requires an expression for $F(r)$ in eq. (3.2). While it is not clear what the proper choice should be, the total energy grows larger with $r$ so the value $r$=2.1 Å is likely to be the most probable value for $r$. Therefore, we consider distributions of the form

$$F(r) = N(a) \cdot e^{-a|r-2.1|} \qquad (4.1)$$

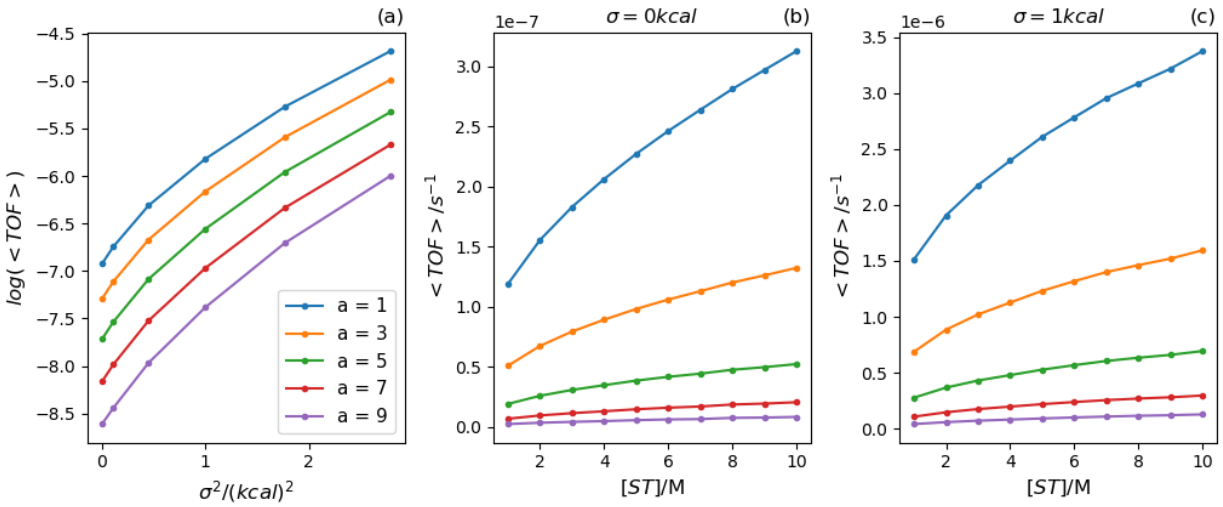


*Figure 7. The TOF averaged over short- and long-range disorder. In panel a, the TOF for T=325K, [$H_2$]=5M, [ST]=1M, and [THF]=0.01M computed for various a values versus $\sigma^2$. In panels b and c, the concentration dependence of TOF at various a values computed for $\sigma$=0 and 1 kcal/mol, respectively.*

We investigate several values of *a* ranging from a broad (*a* small) to a narrow (*a* large) distribution of short-range structure. The average TOF at fixed [ST], [$H_2$], and [THF] was computed using 500,000 noise values as a function of *r*, and then integrated over *r* using eq. (3.2). The TOF at fixed concentration is shown in Fig. 7 for various *a*-values as a function of the strength of noise. The *r*-averaging clearly preserves the noise enhancement of the rate seen for the fixed *r*-results. The fully averaged TOF as functions of [ST] for various *a* values (in units of $Å^{-1}$) choosing the noise parameter of $\sigma$=1 kcal/mol is shown in Fig. 7c. It is seen that the TOF shows weak saturation behavior versus [ST] for all *a* values. However, the results do not fit well to a linear Lineweaver-Burk plot nor to a linear Hill plot.

# V. Multiple Reaction Pathways and Disorder Explain Nonlinear Lineweaver-Burk Plots

The origin of the nonlinear behavior in Fig. 7 can be traced mostly to reaction path branching which is either promoted or suppressed depending on the values of the disorder parameter *r*. As was seen in Fig. 2, there are three basic catalytic pathways that contribute simultaneously to the complete TOF. It is possible to approximately extract the separate contributions to the kinetics from the individual pathways (5-7) by blocking flux going along the other two paths with artificially high barriers. Thus, the contribution of pathway 7 is found by

setting the barriers for structures **18b** and **18c** to high values. Similarly, pathways 5 and 6 can be isolated by raising the barriers for **18a** and **18c**, and for **18a** and **18b**, respectively. In Fig. 8a, we see how the TOF decomposes into path contributions versus *r* for [THF]=0.01M, [$H_2$] = 5M and [ST]=1M. We see path 7 dominates the TOF up to about *r*=2.4Å, at which point path 5 begins to contribute significantly and path 6 becomes somewhat more important although path 5 is much more important than path 6 at *r*=2.5Å. Thus we see that in a window around *r*=2.45Å the TOF is due to a combination of paths while outside the window a single pathway dominates. To exhibit how the LB plot responds to changes in *r*, in Figs. 8b we show $\frac{1}{\nu}$ vs. $\frac{1}{[ST]}$ at *r*=2.35, 2.4. 2.45, and 2.5Å holding [$H_2$] and [THF] fixed. The LB plot is sometimes linear, such as at *r*=2.30, 2.36, and 2.5Å, but sometimes nonlinear, such as at *r*=2.45Å. In those region of multiple contributing paths, we see nonlinear behavior. Obviously, when broadly averaged over all *r* using *F(r),* the plot remains nonlinear. However, it is interesting to note that the individual paths each exhibit a linear LB curve even at the value *r*=2.45Å as seen in Fig. 8c.

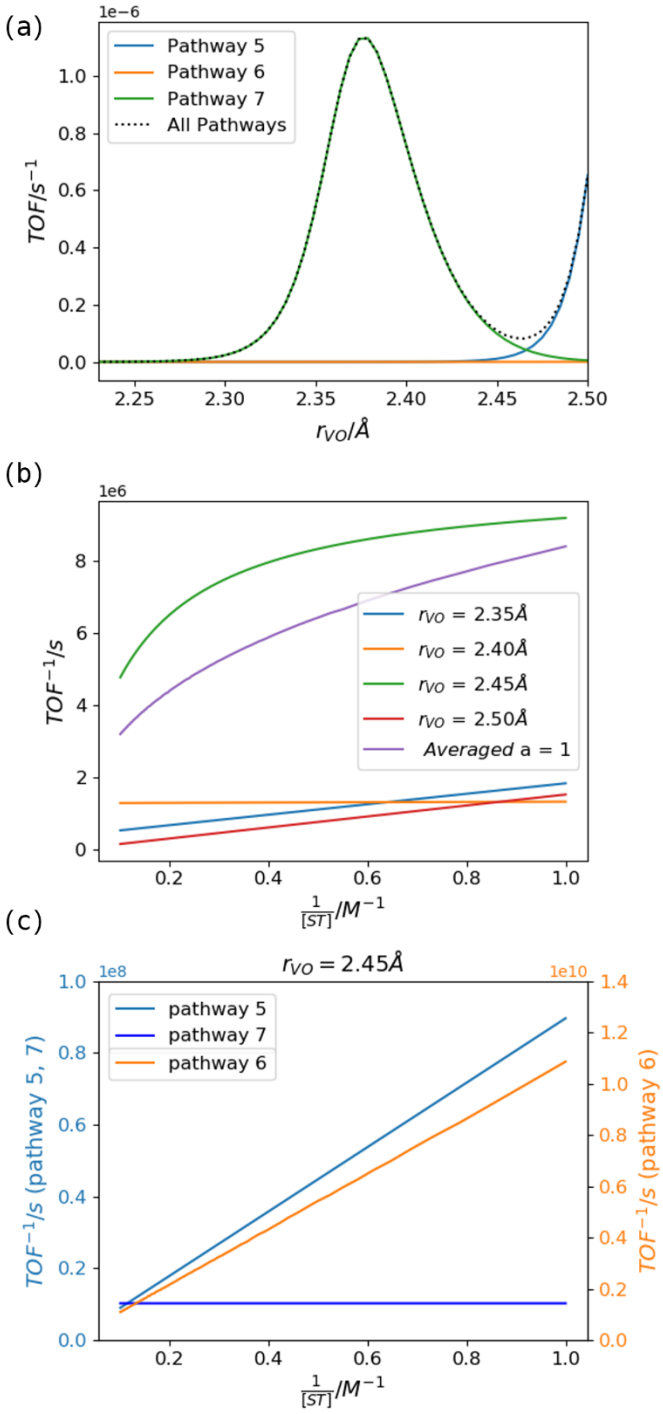


*Figure 8. The pathway analysis of the kinetics for T = 325K, [THF]=0.01M, [ST] = 1M and [$H_2$]=5M. In (a) the TOF versus r is decomposed into contributions from three pathways. In (b) the Lineweaver-Burk plot for various choices of r is shown with the average (observable bulk) value of the LB plot in purple. In (c), the result for r=2.45 Å is decomposed into individual pathways.*

Nonlinear LB curves are commonly seen in branched multi-pathway catalytic networks[56] [71] and in the cooperative kinetics of enzyme catalyzed reactions.[72] [73] In the present problem, even the more general Hill curve remain nonlinear.[56] Here, we also note that disorder can result in nonlinear LB curves even for a purely sequential (single path) reaction mechanism. This may occur since the general sample average of the TOF yields

$$\frac{1}{\nu} = \frac{1}{\sum_q F_q \frac{\nu_{max}^q [S]}{[S] + K_M^q}} \neq A + \frac{B}{[S]} \qquad (5.1)$$

In particular, if the affinity parameter $K_M^q$ shows strong variation over the sample, then the overall LB plot is nonlinear. When a sequential (single path) mechanism is subjected to correlated disorder, then we are effectively combining the turnover from a set of completely different sequential mechanisms. In Fig. 9, this is demonstrated by computing the LB plot for styrene saturation broken down into contributions from each pathway but averaged over disorder with $a$=1 Å$^{-1}$ and $\sigma$=1 kcal/mol. The dominant path 7 shows clear nonlinearly which carries over to the full ensemble averaged result. On the other hand, the linear behavior of path 5 and 6 suggests a very weak dependence of $K_M^q$ on the disorder parameters. Hence, we observe that both multiple pathway kinetics and correlated disorder both contribute to nonlinear LB behavior.

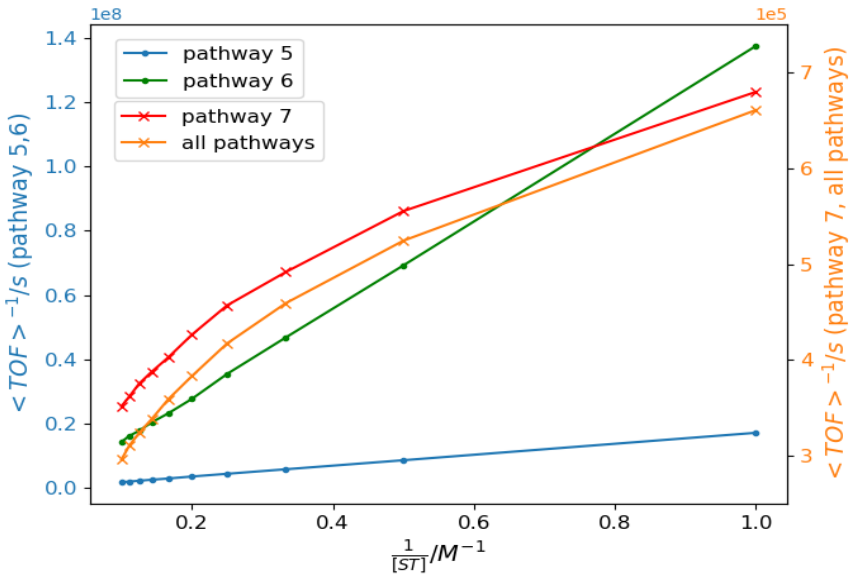


*Figure 8. The Lineweaver-Burk plots for styrene saturation averaged at T=325K, [THF]=0.01M, and [$H_2$]=5M, over the local and global disorder with a=1 Å$^{-1}$ and σ=1 kcal/mol. The pathway decomposed results and full result are shown.*

# VI. Results for Waiting Time Distributions

The TOF is of course only the simplest aspect of the single molecule kinetics, i.e., the first moment of *f(t)*. The full shape of this PDF (eq. 2.13) is vastly more informative since it responds to the full kinetic network. Since a single molecule observation may extract *f(t)* for distinct microscopic environments, it is interesting to investigate how the PDF reflects the disorder. Here we consider just several representative cases for values of the concentrations to illustrate the behavior of *f(t)*. As context, we note that the simple MM scheme $E + S \underset{k_{\pm 1}}{\longleftrightarrow} ES \underset{k_2}{\rightarrow} E + P$ has a well-known analytical solution[33]

$$f(t) = \frac{\lambda_1 \lambda_2}{\lambda_2 - \lambda_1}\left(e^{\lambda_1 t} - e^{\lambda_2 t}\right) \qquad (6.1)$$

where the eigenvalues of $\boldsymbol{T}$ are

$$\lambda_{1,2} = -\frac{k_1[S] + k_{-1} + k_2}{2} \pm \sqrt{\frac{(k_1[S] + k_{-1} + k_2)^2}{4} - k_1 k_2 [S]} \qquad (6.2)$$

This gives rise to a unimodal PDF with a rapid rise in *f(t)* due to transient kinetics ($\lambda_2$) followed by a slower exponential decay set by the rate limiting process ($\lambda_1$). Thus, when [S] is saturated

$f(t) \rightarrow (k_{-1} + k_2)e^{-(k_{-1}+k_2)t}$ and when [S] is small $f(t) \rightarrow (k_1[S]\Gamma)\left(e^{-k_1[S]\Gamma t} - e^{-(k_{-1}+k_2)t}\right)$ where Γ is the branching ratio $\frac{k_2}{k_{-1}+k_2}$. The TOF from the first moment of *f(t)* is consistent with the standard equation (2.1), i.e., $\langle t \rangle = \frac{k_1[S]+k_{-1}+k_2}{k_1 k_2[S]}$, however the maximum $t_{max} = \frac{\ln(\frac{\lambda_1}{\lambda_2})}{\lambda_2-\lambda_1}$ can be significantly smaller than the mean waiting time $< t >$. For general non-defective kinetic networks that exhibit nondegenerate eigenvalues, the PDF is a linear combination $f(t) = \sum c_i e^{\lambda_i t}$ which can be complicated, even showing multimodal behavior as seen by English *et al.*[33] [34]

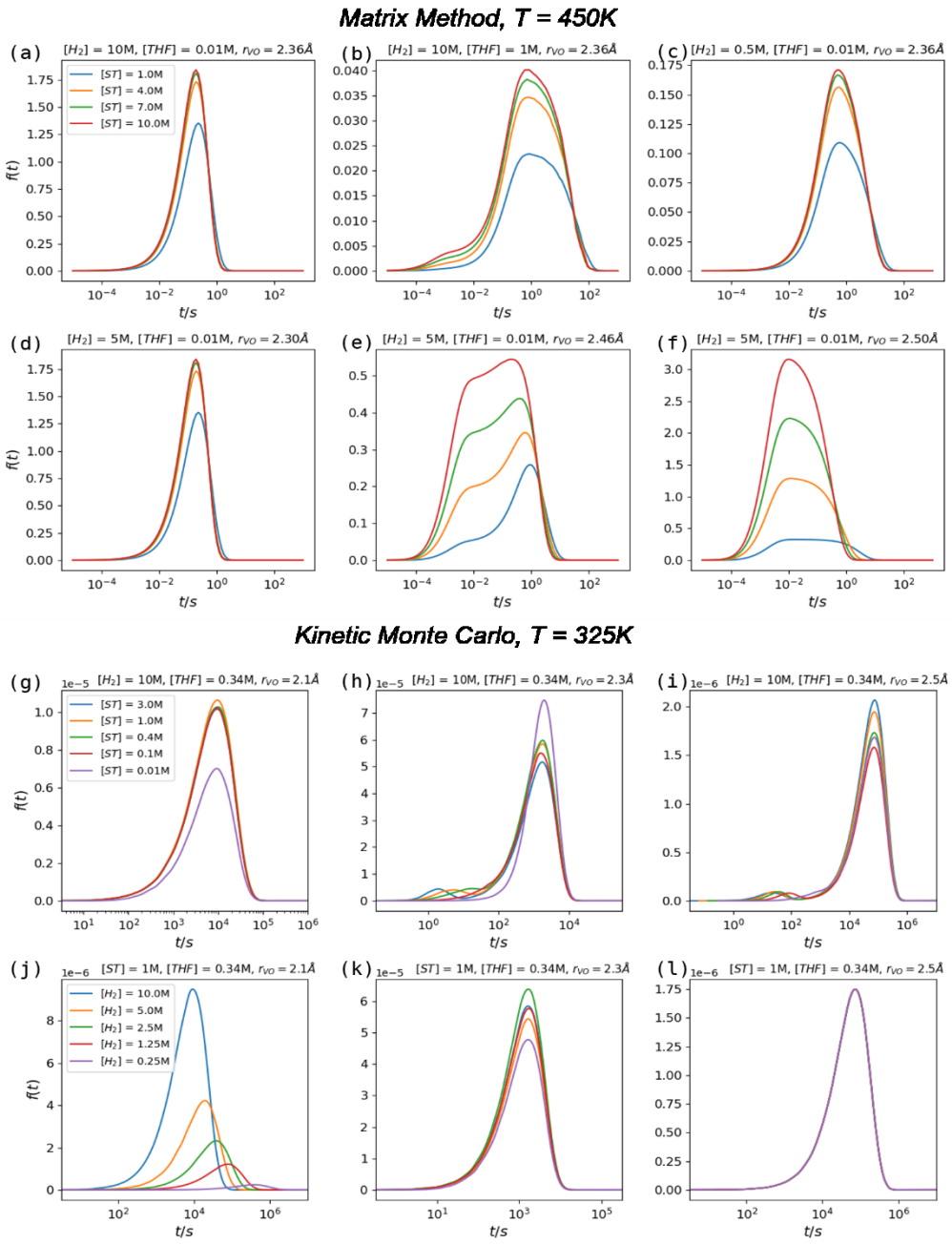


*Figure 10. Waiting time distribution f(t) computed by two different methods. In the upper panels (a)-(f), f(t) is computed by matrix method at T=450K. Panels (a)-(c) demonstrate the [THF] dependence for several [ST] values at r = 2.36 Å and panels (d)-(f) shows the r dependence. In the lower panels, f(t) is computed by kMC at T=325K. The results are for various r, [H₂], and [ST] values with [THF]=0.34M. In all cases the random noise parameter σ is set to zero.*

In Fig. 10, we show *f(t)* on a linear-log scale computed from eq. (2.13) for a survey of catalytic conditions with normalization $\int f(t)dt = 1$. In the upper portion of the figure, *f(t)* is

computed using the MATLAB command EXPM and the temperature was chosen as T=450K to avoid ill-conditioning of exp(***Tt)*** that develops at long times with lower temperatures. For the lower portion of the figure, we employed the slower kMC approach which could be employed at T=325K. In Fig. 10a-c, the PDF is shown for *r*=2.36Å (the optimal value for the TOF) at a number of [ST] values for three levels of the THF inhibitor. In Fig. 10a at low [THF], the PDF is a narrow peak fairly well represented by a two-exponential expression, eq. (6.1). When the concentration of inhibitor increases, as in Figs. 10b and 10c, the peak broadens and develops a clear shoulder for faster turnover times. These are clear signs of multiexponential behavior. The dependence of *f(t)* on [ST] and [$H_2$], highlighted in Figs. 10d-f, is found to be less dramatic than that of [THF]. The peak positions and first moments shift gradually to faster times with increasing concentrations. The most interesting variation in *f(t)* occurs as a function of the disorder parameter *r*. As *r* increases, the shape of *f(t)* clearly evolves and develops two or more distinct features as seen in Figs. 10g-i. This is exciting since it demonstrates a qualitative distinction between different structural environments that is potentially observable in experiment.

The kMC calculations in the lower portion of Fig. 10 were obtained with the quasi-equilibrium approximation invoked for interconversion of the AS's, $AS3 \leftrightarrow AS4 \leftrightarrow AS5$. This allowed *f(t)* to be computed at the lower temperatures 325 K. Although the kMC calculations are time consuming, the instability of the linear equations does not affect the quality of the results. The waiting time distribution were obtained for various substrate concentrations and *r* values with the inhibitor fixed at [THF]=0.34M. The main peak of the PDF in Fig. 10g-l is approximately described by a simple two-exponential representation. However, more complicated structure does develop at shorter turnover times. For example, in Fig. 10h the secondary peak in *f(t)* clearly reflects the contribution of pathway 5 at *r*=2.3Å when pathway 7 is suppressed with the inhibitor. The multi-exponential behavior is intimately connected to the multiple pathway structure.

It is clear that the information contained in *f(t)* goes well beyond what is reflected in the first few moments of the PDF. How can that information be extracted and interpreted? While a full analysis goes beyond our present scope, some aspect of the behavior of *f(t)* can be easily inferred with reference to the catalytic motif shown in Fig. 2. Using the flux blocking scheme introduced in Sec. V, we can analyze the individual pathway contributions to *f(t)* which are computed separately using the ***T***-matrix modified with the high barriers under the conditions

T=450K, [$H_2$]=1M, and [THF]=0.01M. In Fig. 11a, the relative importance of the three pathways is inferred from the TOF versus *r*. It is seen that path 7 constitutes the main contribution to the peak near *r*=2.36Å while influence of pathways 5 and 6 grow significant for larger *r* values, i.e., *r*>2.4Å. In Fig. 11b, the full (unblocked) mechanism PDF for the case *r*=2.45Å is shown which reveals similar structure at all [ST] values. Then in Fig. 11c, the result for [ST]=4M is decomposed into three pathways contributions which sum nearly perfectly to the observed total. The peak near *t*=1 s is due mostly to pathway 7. The feature at shorter times comes from pathway 5. A broad longer time contribution comes from pathway 6. In Figs. 11d-f, the [ST] dependence of separate pathways is exhibited. It is very interesting to note that the [ST] dependence of *f(t)* for pathway 7 is extremely weak. This is due to the fact that styrene attachment along path 7, which occurs after the rate limiting step, has a very low barrier so that it is easily saturated. The takeaway is that the pathway decomposition of the PDF provides a useful tool to unravel the contributions from different reaction routes to the activity of individual reactive sites on a catalyst. To a degree, the resolution of results in time allow the separate pathway structure to be revealed.

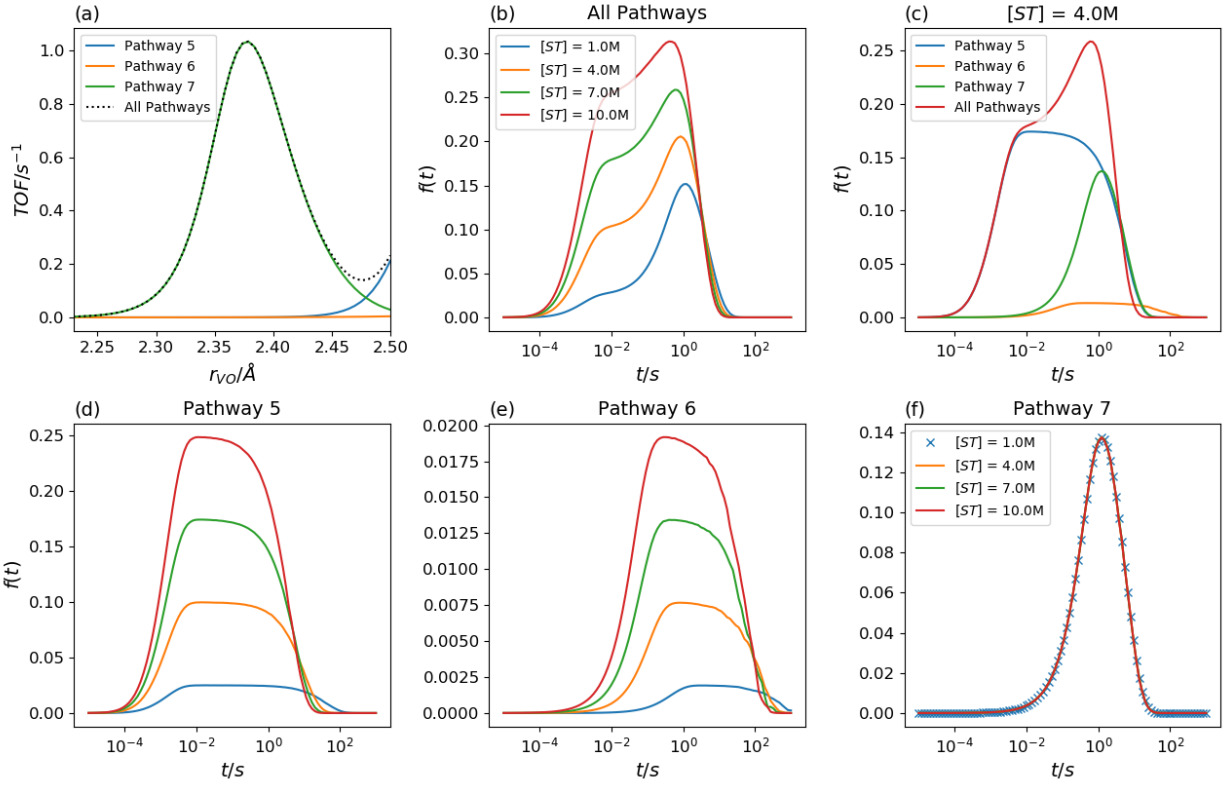


*Figure 11. The pathway analysis of the kinetic mechanism for the case of T=450 K, [THF]=0.01M, and [$H_2$]=5M. In (a) the TOF versus r is decomposed into contributions from three pathways. In (b), the full PDF f(t) is shown for r=2.45Å. In (c), the PDF for*

*r=2.45Å is decomposed into pathway contributions. In (d)-(f), the [ST] dependence of each pathway is shown.*

# VII. Discussion and Conclusions

The single molecule viewpoint is an extremely useful tool to analyze the catalysis of disordered systems. The advantage over the traditional bulk perspective is twofold. First, spatial resolution permits the isolation of turnovers at a single environment of the sample. Second, the temporal resolution allows the kinetics of passage through the network to be spread out in time. As we have shown, the analysis of the waiting time PDF, $f_q(t)$, permits the identification of distinct kinetic pathways as features occurring in different regions of time. Hence, single molecule observations allow us to undo the two averages in the TOF, i.e. $\nu_{obs} = \sum_q F_q \int f_q(t) \cdot t \cdot dt$. The necessary experiments, of course, are very challenging and cannot be routinely applied to systems of interest. However, Chen and coworkers[42-48] have elegantly demonstrated that technology developed previously to study enzymology can be adapted to traditional catalytic systems. Single-atom catalytic systems seem to be a plausible target for experimental study since spatial resolution is possible through use of a sufficiently dispersed sample of catalytic atoms. Of course a successful experiment also requires a spectroscopic signal to monitor the turnover events, and this will be system dependent. We believe that the methods outlined in this paper may provide some guidance in the design and analysis experiments arising from single site catalysts on disorder surfaces.

The present work employs a realistic model based on DFT to study the styrene hydrogenation process with a single site organovanadium catalyst on an amorphous silica support. It was found there are three interconverting active sites that yield three interconnect catalytic cycles. The TOF and $f_q(t)$ may be efficiently extracted from the kinetic model using an SVD representation. This enables large scale simulations of structural disorder implicit in this class of catalysts. Traditional models of disordered kinetics have typically employed random sampling to determine the required reaction barriers. When multiple steps are present in the reaction mechanism, one must face the issue of how the successive reaction barriers correlate to one another. The structural static disorder was divided into two components that had different statistical characteristics. The short-range disorder was modeled by a parameterization of the local structure around the anchoring site of the vanadium atoms to the silica surface. This local structure

gives rise to strong correlation between the reaction barriers along the three catalytic cycles. The long-range disorder models the bulk silica substrate and has a much lower level of correlation between the barriers and is simply represented as Gaussian noise.

The present study represents the first step in the treatment of the supported organovanadium catalyst. We have treated the local structural disorder using only a single geometrical parameter, the V-O bond length. While the local covalent structure imposes severe constraints on the dimensionality of disorder, we anticipate that further parameters will likely be required to fully account for the distribution of active site environments. We must also address the question of proper choice for the statistical probability function *F(r)* that develops from the actual pre-catalyst. It is difficult to use direct experimental data to extract the structural information about site distributions. A purely theoretical approach will require a large number of QM calculations to represent the local environment of the reaction center and scheme to represent the grafting and preparation kinetics. We note that Kahn *et al.*[74] and Vandervelden *et al.*[75] have suggested an "importance learning method" that starts from a quenched disorder parameterized model of silica and aims to make predictions based on a relatively small set of training data. This approach may reduce the number of calculations required. Finally, in the future we shall require a more complete model to relate the weighting time distribution to chemical pathways. Here, we have adopted a rather crude method of pathway selection via flux blocking. It is possible to use a more sophisticated deconvolution method[76-81] to analyze the reaction network that does not involve any alteration of the barrier heights. This will be the subject of future work.

## Acknowledgements

This work was supported by the National Science Foundation through grant CHE1664555. This work was also supported by the U.S. Department of Energy (DOE) Office of Basic Energy Sciences, Division of Chemical Sciences, Geosciences, and Biosciences, Catalysis Science Program under Contract DE-AC02-06CH11357 (Argonne National Laboratory).

TOC-graphic

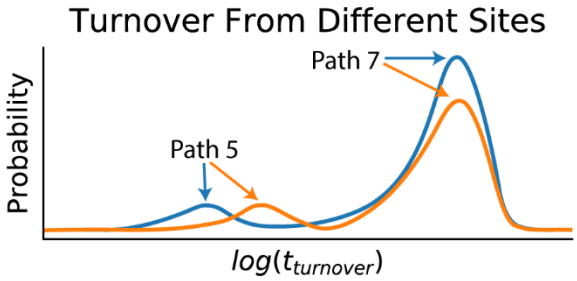


References

[1] Bray, J. M.; Schneider, W. F. First-Principles Analysis of Structure Sensitivity in NO Oxidation on Pt. *ACS Catal.* **2015**, *5* (2), 1087–1099.
[2] Stamatakis, M.; Chen, Y.; Vlachos, D. G. First-Principles-Based Kinetic Monte Carlo Simulation of the Structure Sensitivity of the Water-Gas Shift Reaction on Platinum Surfaces. *J. Phys. Chem. C* **2011**, *115* (50), 24750–24762..
[3] Li, H.; Evans, E. J.; Mullins, C. B.; Henkelman, G. Ethanol Decomposition on Pd-Au Alloy Catalysts. *J. Phys. Chem. C* **2018**, *122* (38), 22024–22032.
[4] Holby, E. F.; Wu, G.; Zelenay, P.; Taylor, C. D. Structure of Fe-Nx-C Defects in Oxygen Reduction Reaction Catalysts from First-Principles Modeling. *J. Phys. Chem. C* **2014**, *118* (26), 14388–14393.
[5] Lang, S. M.; Bernhardt, T. M. Gas Phase Metal Cluster Model Systems for Heterogeneous Catalysis. *Physical Chemistry Chemical Physics*. **2012**, *14*(26), 9255–9269.
[6] Zhang, Z.; Su, J.; Matias, A. S.; Gordon, M.; Liu, Y. S.; Guo, J.; Song, C.; Dun, C.; Prendergast, D.; Somorjai, G. A.; *et al*.. Enhanced and Stabilized Hydrogen Production from Methanol by Ultrasmall Ni Nanoclusters Immobilized on Defect-Rich h-BN Nanosheets. *Proc. Natl. Acad. Sci. U. S. A.* **2020**, *117* (47), 29442–29452.
[7] Andersen, M.; Plaisance, C. P.; Reuter, K. Assessment of Mean-Field Microkinetic Models for CO Methanation on Stepped Metal Surfaces Using Accelerated Kinetic Monte Carlo. *J. Chem. Phys.* **2017**, *147* (15), 152705.
[8] Taylor, H. S. A theory of the catalytic surface. *Proceedings of the Royal Society of London. Series A, Containing Papers of a Mathematical and Physical Character* 1925, *108*(745), 105-111.
[9] Halsey, G. D. Catalysis on Non-Uniform Surfaces. *J. Chem. Phys.* **1949**, *17* (9), 758–761.
[10] Boudart, M.; Djéga-Mariadassou, G. *Kinetics of heterogeneous catalytic reactions*; Princeton University Press: Princeton, NJ, 2014.
[11] Thomas, J. M. The Societal Significance of Catalysis and the Growing Practical Importance of Single-Site Heterogeneous Catalysts. In *Proceedings of the Royal Society A: Mathematical, Physical and Engineering Sciences*; **2012**; *468*, 1884–1903.
[12] Schweitzer, N. M.; Hu, B.; Das, U.; Kim, H.; Greeley, J.; Curtiss, L. A.; Stair, P. C.; Miller, J. T.; Hock, A. S. Propylene Hydrogenation and Propane Dehydrogenation by a Single-Site $Zn^{2+}$ on Silica Catalyst. *ACS Catal.* **2014**, *4* (4), 1091–1098.
[13] Peters, B.; Scott, S. L. Single Atom Catalysts on Amorphous Supports: A Quenched Disorder Perspective. *J. Chem. Phys.* **2015**, *142* (10), 104708.
[14] Goldsmith, B. R.; Peters, B.; Johnson, J. K.; Gates, B. C.; Scott, S. L. Beyond Ordered Materials: Understanding Catalytic Sites on Amorphous Solids. *ACS Catal.* **2017**, *7* (11), 7543–7557.
[15] Campbell, C. T. The Degree of Rate Control: A Powerful Tool for Catalysis Research. *ACS Catal*. **2017**, 2770–2779.
[16] Tian, H.; Rangarajan, S. Computing a Global Degree of Rate Control for Catalytic Systems. *ACS Catal.* **2020**, *10* (22), 13535–13542.
[17] Zádor, J.; Zsély, I. G.; Turányi, T. Local and Global Uncertainty Analysis of Complex Chemical Kinetic Systems. *Reliab. Eng. Syst. Saf.* **2006**, *91* (10–11), 1232–1240.

[18] Zhou, D. D. Y.; Davis, M. J.; Skodje, R. T. Multitarget Global Sensitivity Analysis of N-Butanol Combustion. *J. Phys. Chem. A* **2013**, *117* (17), 3569–3584.
[19] Dumesic, J. A. Analyses of Reaction Schemes Using De Donder Relations. *J. Catal.* **1999**, *185* (2), 496–505.
[20] Schumacher, C.; Gonzalez, J.; Wright, P. A.; Seaton, N. A. Generation of Atomistic Models of Periodic Mesoporous Silica by Kinetic Monte Carlo Simulation of the Synthesis of the Material. *J. Phys. Chem. B* **2006**, *110* (1), 319–333.
[21] Goldsmith, B. R.; Sanderson, E. D.; Bean, D.; Peters, B. Isolated Catalyst Sites on Amorphous Supports: A Systematic Algorithm for Understanding Heterogeneities in Structure and Reactivity. *J. Chem. Phys.* **2013**, *138* (20), 204105.
[22] Patel, P.; Wells, R.; Kaphan, D.; Delferro, M.; Skodje, R. T.; Liu, C. Computational Investigation of the Role of Active Site Heterogeneity for a Supported Organovanadium(iii) Hydrogenation Catalyst, *ACS Catal.* **2021,** 11(12), 7257-7269.
[23] Moerner, W. E.; Kador, L. Optical Detection and Spectroscopy of Single Molecules in a Solid. *Phys. Rev. Lett.* **1989**, *62* (21), 2535–2538.
[24] Moerner, W. E.; Fromm, D. P. Methods of Single-Molecule Fluorescence Spectroscopy and Microscopy. *Review of Scientific Instruments* **2003**, *74* (8), 3597–3619.
[25] Single-Molecule Biophysics: Experiment and Theory, ed. T. Tomatsuzaki, T.; Kawakami, M.; Takahashi, S.; Yang, H.; Silbey, R. J. Advances in Chemical Physics Vol. *146* (John Wiley & Sons, Hoboken, N. J., 2012).
[26] Xie, X. S.;Trautman, J. K. Optical studies of single molecules at room temperature. *Annu. Rev. Phys. Chem.* **1998**, *283,* 1670-1676.
[27] Cornish, P. V.; Ha, T. A Survey of Single-Molecule Techniques in Chemical Biology. *ACS Chemical Biology*, **2007**, *2*(1), 53–61.
[28] Lu, H. P.; Xun, L.; Xie, X. S. Single-Molecule Enzymatic Dynamics. *Science* **1998**, *282* (5395), 1877–1882.
[29] Zhuang, X.; Bartley, L. E.; Babcock, H. P.; Russell, R.; Ha, T.; Herschlag, D.; Chu, S. A Single-Molecule Study of RNA Catalysis and Folding. *Science* **2000**, *288* (5473), 2048–2051.
[30] Noji, H.; Yasuda, R.; Yoshida, M.; Kinosita, K. Direct Observation of the Rotation of F1-ATPase. *Nature* **1997**, *386* (6622), 299–302.
[31] Schnitzer, M. J.; Block, S. M. Statistical Kinetics of Processive Enzymes. In *Cold Spring Harbor Symposia on Quantitative Biology* **1995**, *60*, 793–802.
[32] Shaevitz, J. W.; Block, S. M.; Schnitzer, M. J. Statistical Kinetics of Macromolecular Dynamics. *Biophys. J.* **2005**, *89* (4), 2277–2285.
[33] English, B. P.; Min, W.; Van Oijen, A. M.; Kang, T. L.; Luo, G.; Sun, H.; Cherayil, B. J.; Kou, S. C.; Xie, X. S. Ever-Fluctuating Single Enzyme Molecules: Michaelis-Menten Equation Revisited. *Nat. Chem. Biol.* **2006**, *2* (2), 87–94.
[34] Kou, S. C.; Cherayil, B. J.; Min, W.; English, B. P.; Xie, X. S. Single-Molecule Michaelis-Menten Equations. **2005**. *109 (41),* 19068-19081.
[35] Chemla, Y. R.; Moffitt, J. R.; Bustamante, C. Exact Solutions for Kinetic Models of Macromolecular Dynamics. *J. Phys. Chem. B* **2008**, *112* (19), 6025–6044.
[36] Cao, J.; Silbey, R. J. Generic Schemes for Single-Molecule Kinetics. 1: Self-Consistent Pathway Solutions for Renewal Processes. *J. Phys. Chem. B* **2008**, *112* (41), 12867–12880.
[37] Roussel, M. R. The Use of Delay Differential Equations in Chemical Kinetics. *J. Phys. Chem.* **1996**, *100* (20), 8323–8330.
[38] Cao, J. Michaelis-Menten Equation and Detailed Balance in Enzymatic Networks. *J. Phys. Chem. B* **2011**, *115* (18), 5493–5498.
[39] Ninio, J. Alternative to the Steady-State Method: Derivation of Reaction Rates from First-Passage Times and Pathway Probabilities. *Proc. Natl. Acad. Sci. U. S. A.* **1987**, *84* (3), 663–667.
[40] Zhang, X. J.; Qian, H.; Qian, M. Stochastic Theory of Nonequilibrium Steady States and Its Applications. Part I. *Physics Reports* **2012**, *510* (1-2), 1–86.
[41] Ge, H.; Qian, M.; Qian, H. Stochastic Theory of Nonequilibrium Steady States. Part II: Applications in Chemical Biophysics. *Physics Reports* **2012**, *510* (3), 87–118.
[42] Xu, W.; Kong, J. S.; Yeh, Y. T. E.; Chen, P. Single-Molecule Nanocatalysis Reveals Heterogeneous Reaction Pathways and Catalyticdynamics. *Nat. Mater.* **2008**, *7* (12), 992–996.
[43] Han, K. S.; Liu, G.; Zhou, X.; Medina, R. E.; Chen, P. How Does a Single Pt Nanocatalyst Behave in Two Different Reactions? A Single-Molecule Study. *Nano Lett.* **2012**, *12* (3), 1253–1259.
[44] Andoy, N. M.; Zhou, X.; Choudhary, E.; Shen, H.; Liu, G.; Chen, P. Single-Molecule Catalysis Mapping Quantifies Site-Specific Activity and Uncovers Radial Activity Gradient on Single 2D Nanocrystals. *J. Am. Chem. Soc.* **2013**, *135* (5), 1845–1852.

[45] Shen, H.; Zhou, X.; Zou, N.; Chen, P. Single-Molecule Kinetics Reveals a Hidden Surface Reaction Intermediate in Single-Nanoparticle Catalysis. *J. Phys. Chem. C* **2014**, *118* (46), 26902–26911.
[46] Chen, P.; Zhou, X.; Andoy, N. M.; Han, K. S.; Choudhary, E.; Zou, N.; Chen, G.; Shen, H. Spatiotemporal Catalytic Dynamics within Single Nanocatalysts Revealed by Single-Molecule Microscopy. *Chem. Soc. Re*. **2014**, *43* (4), 1107–1117.
[47] Chen, T.; Chen, S.; Song, P.; Zhang, Y.; Su, H.; Xu, W.; Zeng, J. Single-Molecule Nanocatalysis Reveals Facet-Dependent Catalytic Kinetics and Dynamics of Pallidium Nanoparticles. *ACS Catal.* **2017**, *7* (4), 2967–2972.
[48] Ye, R.; Mao, X.; Sun, X.; Chen, P. Analogy between Enzyme and Nanoparticle Catalysis: A Single-Molecule Perspective. *ACS Catal.* **2019**, *9* (3), 1985–1992.
[49] Witzke, R. J.; Chapovetsky, A.; Conley, M. P.; Kaphan, D. M.; Delferro, M. Nontraditional Catalyst Supports in Surface Organometallic Chemistry. *ACS Catal*. **2020**, *10* (20), 11822–11840.
[50] Sohn, H.; Camacho-Bunquin, J.; Langeslay, R. R.; Ignacio-De Leon, P. A.; Niklas, J.; Poluektov, O. G.; Liu, C.; Connell, J. G.; Yang, D.; Kropf, J *et al*. Isolated, Well-Defined Organovanadium(III) on Silica: Single-Site Catalyst for Hydrogenation of Alkenes and Alkynes. *Chem. Commun.* **2017**, *53* (53), 7325–7328.
[51] Kaphan, D. M.; Ferrandon, M. S.; Langeslay, R. R.; Celik, G.; Wegener, E. C.; Liu, C.; Niklas, J.; Poluektov, O. G.; Delferro, M. Mechanistic Aspects of a Surface Organovanadium(III) Catalyst for Hydrocarbon Hydrogenation and Dehydrogenation. *ACS Catal.* **2019**, *9* (12), 11055–11066.
[52] Islam, M. M.; Costa, D.; Calatayud, M.; Tielens, F. Characterization of Supported Vanadium Oxide Species on Silica: A Periodic DFT Investigation. *J. Phys. Chem. C* **2009**, *113* (24), 10740–10746.
[53] Liu, C.; Camacho-Bunquin, J.; Ferrandon, M.; Savara, A.; Sohn, H.; Yang, D.; Kaphan, D. M.; Langeslay, R. R.; Ignacio-de Leon, P. A.; Liu, S *et al.* Development of Activity–Descriptor Relationships for Supported Metal Ion Hydrogenation Catalysts on Silica. *Polyhedron* **2018**, *152*, 73–83.
[54] Quadrelli, E. A.; Basset, J. M. On Silsesquioxanes' Accuracy as Molecular Models for Silica-Grafted Complexes in Heterogeneous Catalysis. *Coordination Chemistry Reviews* **2010**, *254*(5-6), 707–728.
[55] Briggs, G. E.; Haldane, J. B. S. A Note on the Kinetics of Enzyme Action. *Biochem. J.* **1925**, *19* (2), 338–339.
[56] Cornish-Bowden, A. *Fundamentals of Enzyme Kinetics*; Portland Press Ltd.: London, 2004.
[57] Christiansen, J. A., The Elucidation of Reaction Mechanisms by the Method of Intermediates in Quasi-Stationary Concentrations. *Adv. Catal.* **1953**, *5*, 311.
[58] Kozuch, S.; Shaik, S. A Combined Kinetic-Quantum Mechanical Model for Assessment of Catalytic Cycles: Application to Cross-Coupling and Heck Reactions. *J. Am. Chem. Soc.* **2006**, *128* (10), 3355–3365.
[59] Wang, A.; Li, J.; Zhang, T. Heterogeneous Single-Atom Catalysis. *Nat. Rev.Chem.* **2018**, *5* (22), 65–81.
[60] Van Kampen, N. G. *Stochastic Processes in Physics and Chemistry*, 3rd ed.; Elsevier: Amsterdam, 2007
[61] Neuts, M. F. *Matrix-geometric solutions - An algorithmic approach*; The Johns Hopkins University Press: Baltimore, MD, 1981.
[62] Gillespie, D. T.; Hellander, A.; Petzold, L. R. Perspective: Stochastic Algorithms for Chemical Kinetics. *J. Chem. Phys.* **2013**, *138* (17), 170901.
[63] Stoltze, P. Microkinetic Simulation of Catalytic Reactions. *Progress in Surface Science* **2000**, *65* (3-4), 65–150.
[64] Frisch, M. J.; *et al*. *Gaussian 16*, rev.C.01; Gaussian, Inc.: Wallingford, CT, 2016.
[65] Becke, A. D. Density-functional thermochemistry. III. The role of exact exchange. *J. Chem. Phys.* **1993**, *98* (7), 5648-5652.
[66] Lee, C.; Yang, W.; Parr, R. G. Development of the Colle-Salvetti Correlation-Energy Formula into a Functional of the Electron Density. *Phys. Rev. B* **1988**, *37* (2), 785–789.
[67] Stevens, W. J.; Basch, H.; Krauss, M. Compact Effective Potentials and Efficient Shared-Exponent Basis Sets for the First- and Second-Row Atoms. *J. Chem. Phys.* **1984**, *81* (12), 6026–6033.
[68] Stevens, W. J.; Krauss, M.; Basch, H.; Jasien, P. G. Relativistic Compact Effective Potentials and Efficient, Shared-Exponent Basis Sets for the Third-, Fourth-, and Fifth-Row Atoms. *Can. J. Chem.* **1992**, *70* (2), 612–630.
[69] Cundari, T. R.; Stevens, W. J. Effective Core Potential Methods for the Lanthanides. *J. Chem. Phys.* **1993**, *98* (7), 5555–5565.
[70] Schäfer, A.; Huber, C.; Ahlrichs, R. Fully Optimized Contracted Gaussian Basis Sets of Triple Zeta Valence Quality for Atoms Li to Kr. *J. Chem. Phys.* **1994**, *100* (8), 5829–5835.
[71] Hill, T. L. *Free Energy Transduction and Biochemical Cycle Kinetics*; Springer Verlag: New York, 1989.
[72] Cornish-Bowden, A.; Cardenas, M. L. Cooperativity in Monomeric Enzymes *J. Theor. Biol.* **1987**, *124*, 1-23.
[73] Wu, J.; Cao, J. Generalized Michaelis-Menten Equation for Conformational Modulated Monomeric Enzymes. *Adv. Chem. Phys.* **2012,** *146* 329-366.
[74] Kahn, S. A.; Vanderveldon, C. A.; Scott, S. L.; Peters, B. Grafting Metal Complexes Onto Amorphous Supports: From Elementary Steps to Catalyst Site Populations *via* Kernel Regression. *React. Chem. Eng.* (**2020**) **5**, 66-76.

[75] Vandeveldon, C. A.; Kahn, S. A.; Scott, S. L.; Peters, B. Site-Averaged Kinetics for Catalysts on Amorphous Supports: A Learning Algorithm. *React. Chem. Eng*. **2020**, *5*, 77-86.
[76] Bai, S.; Skodje, R. T. The Sum over Histories Representation for Chemical Kinetics: A Quantitative Theory Based on Chemical Pathways. *Int. Rev. Phys. Chem.* **2016**, *35* (4), 539–567.
[77] Bai, S.; Zhou, D.; Davis, M. J.; Skodje, R. T. Sum over Histories Representation for Chemical Kinetics. *J. Phys. Chem. Lett.* **2015**, *6* (1), 183–188.
[78] Bai, S.; Davis, M. J.; Skodje, R. T. Sum over Histories Representation for Kinetic Sensitivity Analysis: How Chemical Pathways Change When Reaction Rate Coefficients Are Varied. **2015**, *119*, 11039-11052.
[79] Wells, R. H.; Gu, X. K.; Li, W. X.; Skodje, R. T. Understanding Surface Catalyzed Decomposition Reactions Using a Chemical Pathway Analysis. *J. Phys. Chem. C* **2018**, *122* (49), 28158–28172.
[80] Bai, S.; Skodje, R. T. Simulating Chemical Kinetics Without Differential Equations: A Quantitative Theory Based on Chemical Pathways. *J. Phys. Chem. Lett.* **2017**, *8* (16), 3826–3833.
[81] Bai, S.; Davis, M. J.; Sivaramakrishnan, R.; Skodje, R. T. A Chemical Pathway Perspective on the Kinetics of Low-Temperature Ignition of Propane. *Combust. Flame* **2019**, *202*, 154–178.